Combustion and Flame 180 (2017) 158–166

Contents lists available at ScienceDirect

Combustion and Flame

journal homepage: www.elsevier.com/locate/combustflame

Multi-parameter measurements of laminar sooting flames using thermophoretic sampling technique

Zuwei Xu, Haibo Zhao*, Xiaobing Chen, Chun Lou*

State Key Laboratory of Coal Combustion, School of Energy and Power Engineering, Huazhong University of Science and Technology, Luoyu Road 1037, Wuhan 430074, China

ARTICLE INFO

Article history:
Received 26 September 2016
Revised 13 December 2016
Accepted 1 March 2017

Keywords:
Thermophoretic sampling
Soot volume fraction
Particle size distribution
Flame temperature
Flow velocity

ABSTRACT

The dual exposure-time thermophoretic sampling (DTTS) method had successfully realized multi-parameter measurements for flame synthesis TiO_2 nanoparticles (Xu and Zhao, 2015), which was further researched and developed to apply to sooting flame diagnosis in this study. However, the traditional sampling probe (TEM grid) cannot satisfy the assumption of convection dominant for heat transfer between probe and flame when moving to a sooting flame that radiation would affect the temperature of the probe dramatically owing to very high emissivity of soot particles. After a comprehensive investigation, we found that the radiative heat transfer between the sampling probe and the sooting flame can be effectively eliminated when tailor-made ultrathin quartz glass slices (UQGSs) were used as novel sampling probes due to a very low emissivity of UQGSs (high radiative transparency). Thereby the interaction between the flame and the UQGS probe conformed to an experiential convective heat transfer - thermophoresis coupling mechanism. As the amount of particles deposited on the probe surface by thermophoresis was a function of soot volume fraction, probe exposure time, gas temperature and flow velocity, two thermophoresis samplings with different exposure time (one is far less than the time constant τ of the UQGS and another is close to τ) in a same position were conducted to simultaneously measure soot volume fraction and flow velocity in the location. The collections of particles with tunable exposure time of probes in the flame were observed and analyzed by a field-emission scanning electron microscope (FESEM) and FESEM-image processing for soot particle size. The novel sampling probe as well as the DTTS technique provided a practical way to perform multivariate measurements of soot volume fraction, flow velocity, and soot particle size distribution.

1. Introduction

Soot, which is a serious environmental pollutant, also affects dramatically heat transfer characteristics of most practical hydrocarbon/air combustion occasions, such as internal combustion engines, gas turbines, boilers, and fires [1-3]. Consequently, it is important to gain a fundamental understanding of the complex sooting processes in flames. Soot particles produced in hydrocarbon flames as results of complicated physical–chemical processes in which gas-to-particle conversion occurs within a very short time scale, of the order of few milliseconds [2,4]. The chemical kinetics are coupled with particle dynamics for sooting processes from micro atomic scale to mesoscopic particulate scale, considering PAH-based inception and surface chemistry (growth and oxidation), coagulation, and fragmentation [5-8]. The experimental and numerical investigations of the fundamental soot evolution, including the soot precursor chemistry, particle nucleation, mass/size growth and ablation, are undoubtedly the mainstream scientific attempts [9-14]. Although many considerable knowledge of the soot phenomenon was obtained over the last two decades, the complete understanding of the chemical and physical mechanisms of the entire process has not been accomplished yet.

The study of soot formation and destruction mechanisms requires reliable measurements of local soot concentrations and particle/aggregate sizes as well as the temperature-time history of soot particles in flames. The properties of soot history include, but are not limited to, temperature, velocity, exposure time, and size distribution of particles. Soot concentrations and particle/aggregate sizes have been investigated extensively in the past decades. In practice, measurements of distributions of temperature and soot volume fraction in flames are essential for the understanding of soot formation. There is a vast literature related to measurements of temperature and soot volume fraction, particularly with non-intrusive in-situ optical diagnostic methods. Light extinction is a

* Corresponding authors.
E-mail addresses: klinsmannzhb@163.com (H. Zhao), lou_chun@sina.com (C. Lou).

http://dx.doi.org/10.1016/j.combustflame.2017.03.003
0010-2180/

path-integrated or line-of-sight technique, which provides field-integrated values of the soot volume fraction [15,16]. Two-color analysis of soot radiative emission is a typical kind of emission technique, which has been used to estimate the average values of soot volume fraction and temperature [17]. Laser-induced incandescence (LII) of soot provides spatially and temporally resolved measurements of soot distribution [18-21]. Multi-wavelength emission measurements have also been employed to measure the spatial distributions of soot temperature and volume fraction [22,23]. However, optical diagnostic techniques, almost without exception, make use of a large number of sophisticated equipment that integrate highly specialized skills and instruments in signal detection, data inversion, information representation [24,25]. These make us have to consider the costs and experimental conditions of research works. Additionally, a calibration procedure, often based on extinction measurements or gravimetric analysis, is normally required.

Recently, a thermocouple thermometer and a thermophoretic probe have been widely used as a calibration-independent technique for absolute flame temperature and particle volume fraction measurements due to less uncertainty. Thermocouple particle densitometry method (TPD) is mainly used in measurement of temperature and soot volume fraction in laminar diffusion flames [26,27]. Although the probe contacts with the flame in the measurement, this method obtains information through the variation of temperature in the probe because of soot deposition. A novel technique is proposed for improvement of the traditional thermocouple measurement recently reported by the current research group [28,29]. The key point of the newly-proposed method is to tailor-make a thermocouple junction that can realize accurate "balance compensation" for heat conduction from the wires, radiation heat loss from the bead, variations of specific heat capacity. There was a time window to maintain invariable thermal inertia coefficient during the initial phase of the thermocouple response.

Measurement and analytical techniques using thermophoretic sampling and transmission electron microscopy (TEM) have greatly improved the knowledge about the properties of soot particles [30]. Thermophoretic sampling is also the most common and easily realized way of collecting particles out of flames, introduced by George et al. [31] and further improved by Dobbins et al. [32] for measuring the size and morphology of soot particles. Köylü et al. [33] proposed the thermophoretic sampling particle diagnostic (TSPD) method based on the theory of particle deposition rate by Eisner and Rosner [27], which can be used to determine not only particle/aggregate size distribution and microstructure but also absolute soot volume fraction. However, the TSPD technique was subject to the following assumptions and restrictions [33]: the gas flow velocity and the probe wall temperature are known constant. In fact, there is spatial distribution of gas flow velocity even in a steady flame, with exact numbers not known in advance, and the temperature of the probe changes over the exposure time in the flame due to heat transfer.

The exposure time of soot particle is directly dependent on stream velocity. The increased stream velocity in the normal flame may reduce the exposure time for soot formation in coflow flames, resulting in a reduction of soot emissions [34]. Therefore, flow velocity is critical to soot dynamic evolution and offers the possibility of studying the fate of soot particles. As known, there is not currently an available measurement solution for flow velocity in sooting flames because most well-developed flow velocity measurements depend on micron-sized tracer particles, such as particle image velocimetry (PIV) [35] and laser Doppler velocimetry (LDV) [34,36]. However, laser-based techniques need expensive dedicated equipment and strongly depend on the tracer particles. In our previous work, multiple internal and external properties of TiO_2 nanoparticles in flame were measured and characterized simultaneously by the dual exposure-time thermophoretic sampling (DTTS) method that used molybdenum TEM grids as thermophoresis probe [28,37]. The DTTS technique is well-established for the analysis of flow velocity.

In this work, the DTTS technique using ultrathin quartz glass slices (UQGSs) as thermophoresis probes to collect soot particles within two different time intervals at one position of flame is proposed, followed by field-emission scanning electron microscope (FESEM) characterization and FESEM-image processing. It should be noted that TEM is not applicable to observe soot particles on the UQGSs, whereas FESEM is a fairly applicable instrument. Since the electron beam passes through the sample that is being examined by TEM, the sample and holder must be sufficiently thin. Usually, samples are supported on a wafer-thin foil (dozens of nanometres thick) of a TEM grid before being loaded into the TEM. Actually UQGS possesses a thickness of 30 μm and therefore electron beams fail to pass through in a TEM. FESEM focuses on the sample's surface and morphology, thereby meeting the requirement of characterizing soot particles on UQGSs. The novel thermophoretic sampling method is a development of TSPD technique to explore the relationship between soot thermophoresis deposition and convection heat transfer of probes, which can simultaneously detect soot volume fraction and flow velocity. The tailor-made DTTS method for multivariate measurement of sooting flame is examined in a benchmark ethylene/air laminar diffusion flame. The experimental measurements of soot volume fraction and stream velocity at different heights above the burner (HABs) are compared with past measurement results as well as the simulation results using a soot model.

2. Experimental

2.1. Apparatus description

In the present experiment, the Gülder burner flame is chosen for the measurement, which is one of three target flames defined by the LII workshop [20]. There is a standardized flame condition of Gülder burner, which can be used for validation and calibration experiments. The burner consists of a fuel nozzle with a 10.9-mm inner diameter, centered in an air tube 100-mm in diameter, and the annulus air region packs with glass beads and porous metal disks to prevent flame instabilities. The ethylene fuel flow rate is set to the smoke point, 0.194 L/min, and the air coflow is 284 L/min [38,39].

The thermophoretic sampler is composed of a double acting high-speed pneumatic cylinder (Festo, DSNU), a programmable logic controller (PLC), a self-closing tweezers, a well-designed sampling probe — ultrathin quartz glass slice (UQGS, presented in Fig. S1 of the supplementary material (SM)) and other auxiliaries. Figure 1 shows a sketch of this thermophoresis sampler. The pneumatic rod end of the double acting cylinder is connected with the self-closing tweezers, carrying the UQGS to the intended sampling positions for an intended exposure time (t_e). When an UQGS is rapidly inserted into the pre-specified sampling position by the high-speed pneumatic cylinder, nearby soot particles will deposit on the UQGS surface due to thermophoresis, meanwhile the temperature of UQGS will increase due to heat transfer from the flame. The timer function of the PLC is used to determine and control the exposure time at the sampling locations, which can ensure representative sampling and avoid overlapping aggregates on the UQGS (The discussion is presented in SM Section 1). After this sampling process, the central zone of the UQGS with an area less than 0.01 mm^2 is observed by FESEM to separate the soot samples at the target point, same as the authors' previous method [28].

The UQGS possesses ultrathin structure with a diameter of 3 mm and a thickness of 30 μm, which benefits minimizing the disturbance to sooting flame. The manufacture of the UQGSs is based

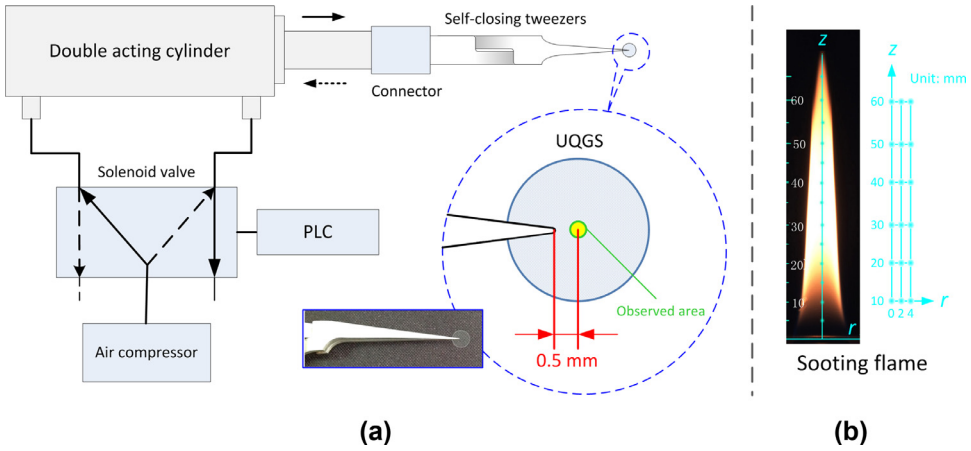

Fig. 1. Schematic of experimental equipment: thermophoretic sampler (a); flame photo and measuring positions (b).

on laser processing: a fused quartz rod is cut into uniform slices and then the slices are polished. The 3-mm diameter depends on the diameter of the perform rod. If necessary, we can use cotton buds drenched by alcohol to wipe the tip of the tweezers. The UQGSs are very suitable for recycling. Used ones can be put into ethanol and cleaned by ultrasonic for 5 min, then dried in an oven.

2.2. Flame temperature measurement

The primary objective of this work is to use thermophoretic sampling technique to measure the soot volume fraction and flame velocity simultaneously. As known, soot thermophoresis is determined by the distribution of temperature, velocity, and particle concentration in the flow boundary layer of thermophoretic probe. The flame temperature is first measured using the tailor-made thermocouple and the dynamic transient method proposed previously by our group [20,28,37]. An uncoated B-type (Pt/Rh 70%/30% - Pt/Rh 94%/6%) fine-wire thermocouple is used to measure the flame temperatures in these intended sampling positions. The junction diameter is 0.7 mm, and the wire diameter is 0.3 mm. The initial short-exposure period of the thermocouple that is well designed to meet the first-order response curve for high-temperature transient measurements. The temperature profiles along the axial line of sooting flame at six specified measuring positions (*i.e.*, $r=0$, $z=10, 20, \ldots, 60$ mm in Fig. 1) were obtained in our previous work [28]. In this work, we further measure the radial temperatures (*i.e.*, $r=0, 2, 4$ mm) at six HABs and then attain two-dimensional temperature profiles of the flame using the dynamic transient method. Using this technique, the measurement results need not to be corrected for radiation and conduction losses of the thermocouple junction, and the effect of soot deposition on thermocouple can be minimized within a short exposure time.

2.3. Soot volume fraction and flame velocity measurement

The soot volume fraction is calculated as [33]:

$$f_v = \frac{2r_F V_p}{D_T N u A_i t_e}\left[1-\left(\frac{T_u}{T_g}\right)^2\right]^{-1} \tag{1}$$

in which r_F is the radius of UQGS corresponding to the FESEM survey area located in the center of UQGS (here $r_F=0.0015$ m), V_p is the total volume of particles in this survey area (V_p characterization is based on the method detailed in SM Section 3), and $D_T=\frac{3}{4}(1+\frac{\pi}{8}\alpha_{mom})^{-1}\upsilon_g$ is the thermophoresis diffusivity, Nu is Nusselt number in the flow boundary layer of UQGS, A_i is the size of the observing area, T_u is the temperature of the UQGS, T_g is flame temperature in the sampling position, t_e is the exposure time of UQGS in flame, α_{mom} is the momentum accommodation coefficient (1 in this study), υ_g is gas kinematic viscosity. The maximum temperature of the UQGS is approximately 1000 K during sampling process, and the thermal accommodation coefficient of the oxygen-atoms-on-quartz is 0.9 at 1000 K based on the experimental values and numerical values presented by Balat-Pichelin et al. [40] However, the data of the thermal accommodation coefficient is absent at 300–1000 K, and can be inferred in the range of 1.0–0.9. An assumption that the thermal accommodation coefficient is 1.0 leads to the maximum error of 2.8% for soot volume fraction. In this sense, thermal accommodation coefficient of unity is acceptable.

The difficulty of this measurement is how to determine unknown parameters in Eq. (1): Nusselt number Nu and temperature of probe T_u. As mentioned in Introduction, the traditional thermophoretic sampling method is based on earlier works by Köylü and coworkers [33,41]. A copper TEM grid acted as the sampling probe, and a very short exposure time was chosen to prevent overlapping of the soot aggregates. In order to attain Nusselt number and temperature of probe, two assumptions (*i.e.*, the flow velocity of 1 m/s and the steady TEM grid temperature of 350 K [33]) were adopted. Actually, the presence of convection and radiation heat transfer has a significant effect on the temperature of sampling probe, and the flow velocities with spatial non-uniform distribution need to be measured.

It should be noted that conduction is very weak and can be ignored due to high thermal contact resistance between UQGS and self-closing tweezers. When only convection and radiation are considered, the analytical expressions of the unsteady heat balance for the UQGS is given in Eq. (2)

$$\frac{\partial T_u}{\partial t} = \underbrace{\frac{h(T_g-T_u)}{\rho_u c_u}\frac{A}{V}}_{\text{convection}} + \underbrace{\frac{\sigma(1-\chi_t-\chi_r)}{\rho_u c_u}\left(\varepsilon_p T_g^4 + T_0^4 - 2T_u^4\right)\frac{A}{V}}_{\text{radiation}} \tag{2}$$

where t is time, h is the convection heat transfer coefficient; ρ_u and c_u are the density and specific heat capacity of quartz glass, respectively; A and V are the heat transfer area and volume of UQGS, respectively, here $A/V=2/\delta$ for a UQGS, δ is the thickness of the UQGS ($\delta=3\times10^{-5}$ m); σ is the Stefan-Boltzmann constant; χ_t and χ_r are the transmittance and reflectance of the UQGS respectively, here being approximated to transparent; ε_p are the emissivity of the soot particles.

When a sampling probe immerged in the flame, the similarity solution of heat convection conforms to parallel flow empirical correlation, and Nusselt number Nu can be expressed as [42]: $Nu=0.332Re^{1/2}Pr^{1/3}$, where Reynold number $Re=u_g r_F/\upsilon_g$, Prandtl number $Pr=\upsilon_g/a_g$, u_g is gas flow velocity, and a_g is gas thermal diffusivity. In addition, the non-dimensional convective heat transfer coefficient Nu is given by $Nu=hr_F/\lambda_g$, where λ_g is gas

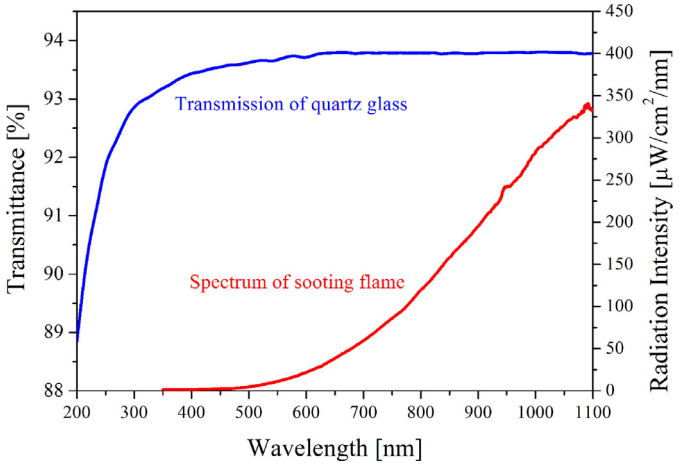

Fig. 2. Spectrum of sooting flame (at a typical height above burner, z=40 mm) and transmission of quartz glass.

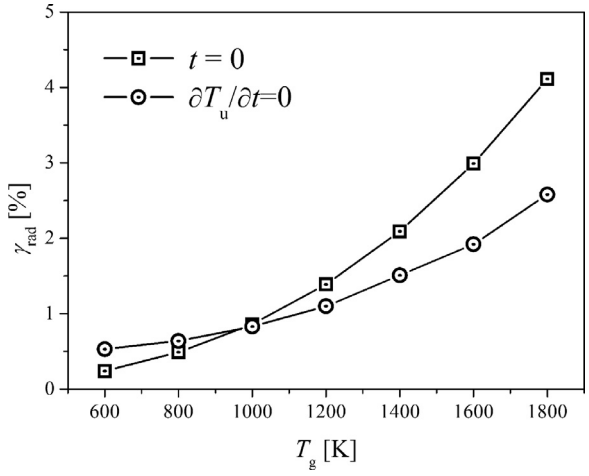

Fig. 3. The ratio of radiation heat flux to total heat flux in the initial state and steady state.

thermal conductivity coefficient. Therefore, the convection heat transfer coefficient h of the UQGS is calculated as:

$$h = 0.332\lambda_g Pr^{1/3} Re^{1/2}/r_F \tag{3}$$

The finite difference technique [43] can be applied to solve Eq. (2), and one of the results is the variables of heat flux by convection and radiation, q_{Conv} and q_{Rad}, respectively. The proportion of radiation heat flux to total heat flux is

$$\gamma_{Rad} = \frac{q_{Rad}}{q_{Conv} + q_{Rad}} \times 100\% \tag{4}$$

As known, quartz glass was often used as optical windows of flame chamber due to its excellent transmittance. With this inspiration, optical quartz glass is used here to make sampling probe, which can provide effective insulation for heat radiation. The spectra of the sooting flame and the transmittance of the UQGS are detected by an optical fiber spectrometer (AvaSpec-2048) with an available wavelength range of 200–1100 nm (cannot be extended further into infrared at present), which is corrected by a blackbody furnace when the temperature of the furnace is at 1000 °C. As shown in Fig. 2, the spectrum of flame is mainly in the visible and infrared light region, in which the intensity increases with the increase of the wavelength. The transmittance of UQGS is up to 93% over the wide spectral region of flame radiation, indicating that the optical quartz glass has a high transparency for visible and infrared light.

As shown in Fig. 3, the calculation results indicate that radiation heat transfer between UQGS and flame can be neglected, not exceeds 5%, and consequently convection heat transfer between UQGS and flame is dominant owing to good radiation transparency of quartz glass from infrared to ultraviolet spectral bands. This result is just pre-estimate before experiment. In this way, we would like to know what the approximate fraction of radiation is and to demonstrate the feasibility of the UQGS method.

Therefore under the condition of ignoring radiation heat transfer and being the dominant mechanism of heat exchange as pure convection, the unsteady energy equation for UQGS is predigested as

$$\frac{\partial T}{\partial t} = \frac{h(T_g - T)}{\rho_u c_u}\frac{A}{V} \tag{5}$$

The solution to Eq. (5) conforms to the first-order response equation

$$T_u = T_0 + (T_g - T_0)[1 - \exp(-t_e/\tau)] \tag{6}$$

where T_0 is the initial temperature (ambient temperature) of the UQGS and τ is the time constant of the UQGS, $\tau = \frac{\rho_u c_u \delta}{2h}$, the convection heat transfer coefficient h is the function of flow velocity u_g in Eq. (3). This means we can determine the temperature of probe in a simple way when the time constant τ is known. In addition, pure convection facilitates the analysis of flow field thereby to implement velocity measurement.

Soot particle deposition in unit area, $\dot{V}_p = V_p/A_i$, is, based on Eq. (1), expressed as

$$\dot{V}_p = \frac{D_T Nu f_v t_e}{2r_F}\left[1 - (T_u/T_g)^2\right] \tag{7}$$

The partial differential form of $\dot{V}_p$ with respect to the exposure time t_e follows

$$d\dot{V}_p = \frac{D_T Nu f_v dt_e}{2r_F}\left[1 - (T_u/T_g)^2\right] \tag{8}$$

The integral form is

$$\dot{V}_p = \int_0^{t_e} d\dot{V}_p = \frac{D_T Nu f_v}{2r_F}\int_0^{t_e}\left[1 - (T_u/T_g)^2\right]dt_e \tag{9}$$

calculated by substituting T_u with Eq. (6):

$$\dot{V}_p = \frac{D_T Nu f_v \tau}{2r_F}\left[2\frac{T_g - T_0}{T_g}\left(1 - e^{-t_e/\tau}\right) + \frac{1}{2}\left(\frac{T_g - T_0}{T_g}\right)^2\left(e^{-2t_e/\tau} - 1\right)\right] \tag{10}$$

In a same position, twice samplings using two fresh UQGS with different exposure time intervals (t_{e1} and t_{e2}) follow Eq. (10), in which the ratio of particle deposition is defined as $\theta = \dot{V}_{p2}/\dot{V}_{p1}$. Because Nu, f_v and τ are constant in a same sampling position, a crucial relationship between two samplings is derived:

$$\theta = \frac{\dot{V}_{p2}}{\dot{V}_{p1}} = \frac{2\frac{T_g - T_0}{T_g}\left(1 - e^{-t_{e2}/\tau}\right) + \frac{1}{2}\left(\frac{T_g - T_0}{T_g}\right)^2\left(e^{-2t_{e2}/\tau} - 1\right)}{2\frac{T_g - T_0}{T_g}\left(1 - e^{-t_{e1}/\tau}\right) + \frac{1}{2}\left(\frac{T_g - T_0}{T_g}\right)^2\left(e^{-2t_{e1}/\tau} - 1\right)} \tag{11}$$

where the time constant τ of the UQGS is the only unknown parameter and can be obtained by solving this equation.

When relating the time constant τ and the convection heat transfer coefficient h in Eq. (3), an explicit formula of flow velocity is available:

$$u_g = r_F\left(\frac{\rho_u c_u \delta}{0.664\tau}\right)^2\sqrt[3]{\frac{\upsilon_g}{\rho_g^2 c_g^2 \lambda_g^4}} \tag{12}$$

where the material properties of gas compositions are functions of temperature. For most properties of each species (C_2H_4, O_2,

N_2, CO_2, H_2O (g), etc.), we define a polynomial, piecewise-linear, or piecewise-polynomial function of temperature using the material databases in Fluent software [26]. For properties of gas mixture, these were composition- and temperature-dependent functions, which can be extracted from the CFD simulation as needed. Finally, the soot volume fraction f_v can be determined according to Eq. (10):

$$f_v = \frac{2r_F\dot{V}_p}{D_T Nu\tau}\left[2\frac{T_g - T_0}{T_g}\left(1 - e^{-t_e/\tau}\right) + \frac{1}{2}\left(\frac{T_g - T_0}{T_g}\right)^2\left(e^{-2t_e/\tau} - 1\right)\right]^{-1} \quad (13)$$

3. Numerical simulations for flow velocity comparison

Since most of the techniques used to study sooting flames do not well suit for flow velocity measurement, no data is available to compare with the flow velocity measured by DTTS approach. Therefore, we conduct numerical simulations using a detailed gas-phase reaction mechanism and complex thermal and transport properties to validate mainly flow velocity measurement. The governing equations of mass, momentum, energy and species in axisymmetric cylindrical coordinates (r, z) given in Ref. [44] are solved in this study. The gravitational term is included in the momentum equation. Correction velocities are used to ensure that the mass fractions sum to unity. The thermophoretic velocities of soot are included in the calculation of the correction velocities. A semi-empirical two-equation formulation is employed to model soot nucleation, growth and oxidation [45], in which C_2H_2 is the only component to manage the inception and growth of the soot. At the same time, soot oxidation by OH radical, O radical and O_2 are considered in the present simulation. SNBCK based wide band model developed by Liu et al. [46] is employed to obtain the absorption coefficients of the combustion products containing CO, CO_2 and H_2O at each wide band. The spectral absorption coefficient of soot is assumed to be $5.5f_v/\lambda$ with f_v being the soot volume fraction and λ the wavelength. The wide bands considered in the calculations are formed by lumping 10 successive uniform narrow bands of 25 cm^{-1}, giving a bandwidth of 250 cm^{-1} for each wide band. The blackbody intensity at each wide band is evaluated at the band center. The radiation source term is calculated by summing up contributions of all the 36 wide bands (from 150 to 9150 cm^{-1}) considered in the calculation.

4. Results and discussion

4.1. Flame temperature

Figure 4 compares the measured profiles with a benchmark experiment by coherent anti-Stokes Raman scattering (CARS) thermometry [16] at r = 0 mm, r = 2 mm, and r = 4 mm for the sooting flame. The measured temperature profiles reproduce previously noninvasive experimental data very well everywhere. The result is fairly satisfactory on the trend of temperature and agrees well with the CARS measurement within relative error of less than 10%. The error bars indicate the precision of the thermocouple measurement is within ±30–50 K.

4.2. Flow velocity

It is well known that insertion of a physical probe into the flame interferes with the flow field and distorts the streamlines. This disturbance is one of the major drawbacks of the thermophoretic sampling technique and its influence on the sampling process is difficult to be quantified [37]. High-speed photographs

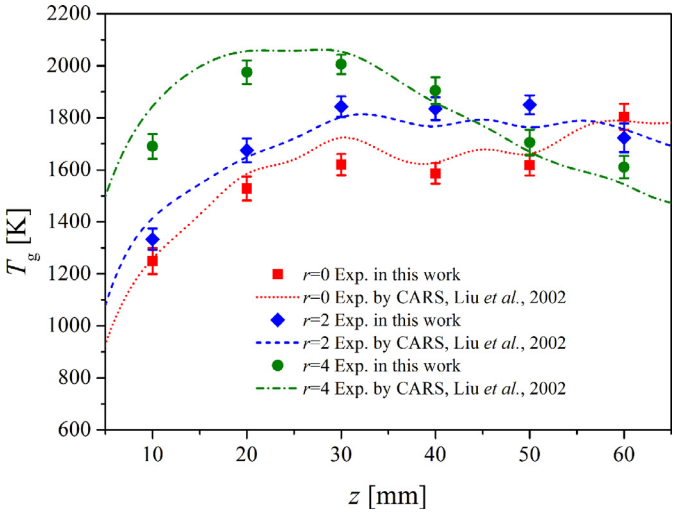

Fig. 4. The measured axial temperature profiles at r = 0 mm, 2 mm and 4 mm for the sooting flame. Error bars are calculated based on five independent measurements.

Table 1
The ratio of particle deposition and time constant for each exposure time.

t_{en} / ms	30	50	80	100	120	150
θ_n	–	1.57	2.32	2.75	3.04	3.39
τ_n / ms	–	109	114	116	110	105
$\Delta\tau_n$ / %	–	1.63	2.89	4.69	0.72	5.24

can provide a direct dissection for this concern in nature. Therefore, we record high-speed images of the flame at 10,000 frames/s using a high-frame rate camera (FASTCAM SA4) during the sampling process. As shown in Fig. S3, a series of images thus captured display several key instantaneous stages while the UQGS probe touches the flame. Throughout the entire process, the flame maintains a relatively stable shape without dramatic distortion, which should be attributed mainly to wafer-thin collector (UQGS) and slender holder (tweezers tip). In addition, Lee et al. [47] recommend an aspect ratio (thickness to width ratio) larger than 0.2 to suppress probe vibration when using a probe with single-arm beam. In this sense, the probe used in the present design employs a tweezers that have two clamping handles, which can effectively prevent probe vibration.

The UQGS traveled through other particle containing regions in the flame before reaching the sampling locations. The travel time (round tripping about 3.0 ms as shown in Fig. S3) was limited to smaller than 10% of the exposure time to minimize the unavoidable contamination during the travel [26,28]. Therefore, the exposure time was not less than 30 ms. Meanwhile, to prevent overlapping of the soot aggregates on the UQGS, 150 ms was almost the upper limit of the exposure time based on FSEM observation. To study the dynamic evolution of soot particle thermophoretic deposition with exposure time, six samplings are carried out at a well-characterized representative location Z40R2 (z=40 mm, r=2 mm) in this flame within different exposure time (t_{e1}, t_{e2},..., t_{e6}): 30 ms, 50 ms, 80 ms, 100 ms, 120 ms, 150 ms. Thereinto, the shortest sampling time t_{e1} = 30 ms is viewed as the reference time. The experimental results of the ratio $\theta_n = \dot{V}_{p,n}/\dot{V}_{p1}$ for these six different sampling time intervals are shown in Fig. 5. When T_0 = 300 K, T_g = 1712 K (at the sampling point Z40R2), and t_{e1} = 30 ms, t_{en} and θ_n are put into Eq. (11) as solved, the time constant τ_n is then obtained (shown in Table 1). The mean and standard deviation of time constant τ_n are $\langle\tau_n\rangle$= 110.8 ms and S_{τ_n}= 4.32, respectively, which indicates that time constant almost keep constant in the

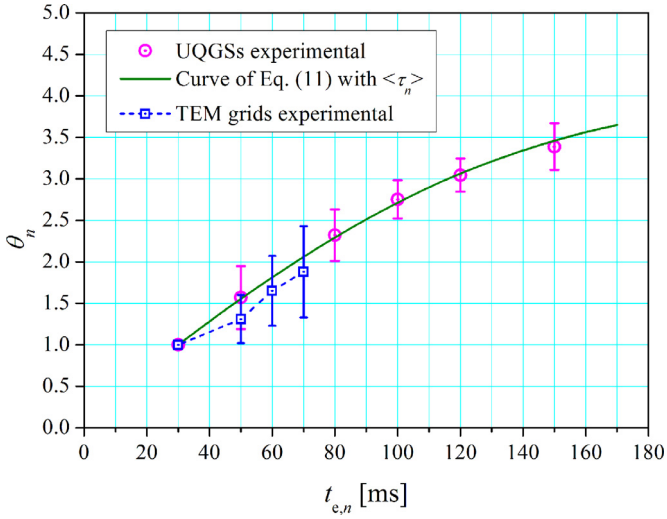

Fig. 5. The ratio of particle deposition at a typical sampling position Z40R2 ($z=40$ mm, $r=2$ mm). Error bars are calculated based on five independent tests of each exposure time.

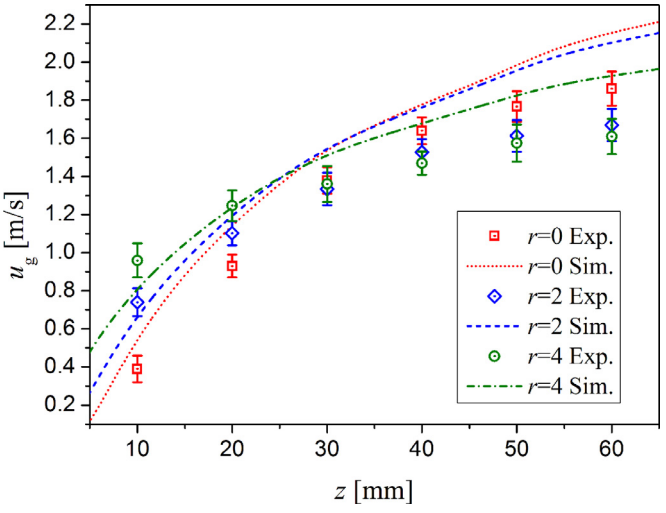

Fig. 6. Evolution of flow velocity (u_g) along the flame height. Error bars are calculated based on five independent tests at each sampling position.

dynamic evolution of soot thermophoretic deposition. Furthermore, the mean time constant $\langle\tau_n\rangle$ is used to draw the dynamic curve, and the curve conforms with these six experimental plots very well. This result demonstrates that particle thermophoretic deposition on the UQGS is mainly dominated by convective heat transfer between the UQGS and flame, and proves the validity and reliability of UQGS as thermophoretic probe considerably.

From the comparison of experimental error bars in Fig. 5 as well as relative deviation $\Delta\tau_n$ ($=\tau_n/\langle\tau_n\rangle \times 100\%$) in Table 1, we find that the net uncertainty values can be minimized when the exposure time t_{e2} approximates to the time constant τ_n based on the fixed t_{e1}. Therefore, two different exposure time, $t_{e1}=30$ ms and $t_{e2}=120$ ms, are determined in this study. Actually we also use TEM grid as thermophoresis probe before UQGS was proposed, however no specific pattern can be followed and thereby the flow velocity cannot be analyzed and obtained. As shown in Fig. 5, the experimental results of TEM grid were added to compare against UQGS measurements. The TEM grid results show that the variations of the ratio θ_n with exposure time distinctly deviate from the assumption of convection dominant due to significant radiation effect. Table S1 indicates that there is a distinct drift in the thermal inertia τ_n of TEM grids. Additionally, the risk that TEM grids are damaged by burning increases with the exposure time. Especially, as the exposure time is over 70 ms in this test, the sampling fails very probably. Therefore, the usage of TEM grid for thermophoresis sampling is recommended for low-radiation flame (*e.g.* TiO_2-laden flame [28,37]).

Flow velocity profiles determined by the DTTS at different HABs are shown in Fig. 6. As there was no published experimental data and results about flow velocity for comparison at present, we use the simulation in Section 3 to evaluate the measurement of flow velocity. The shapes of the profiles are well reproduced by DTTS measurements that exhibit the same tendency as the numerical simulations. Under earth's gravitational environment, buoyancy increases the axial velocities of the combustion species with increasing distance from the burner exit. In our experiment, the flow velocity u_g is calculated from measured T_g and V_p, so the experimental error of u_g is mainly affected by T_g and V_p measurements. It is noted that if the measured T_g is lower (higher) than the actual flame temperature or V_p from FESEM-image analysis is lower (higher) than actual particle deposition, the calculated results of u_g will be higher (lower) than actual performance.

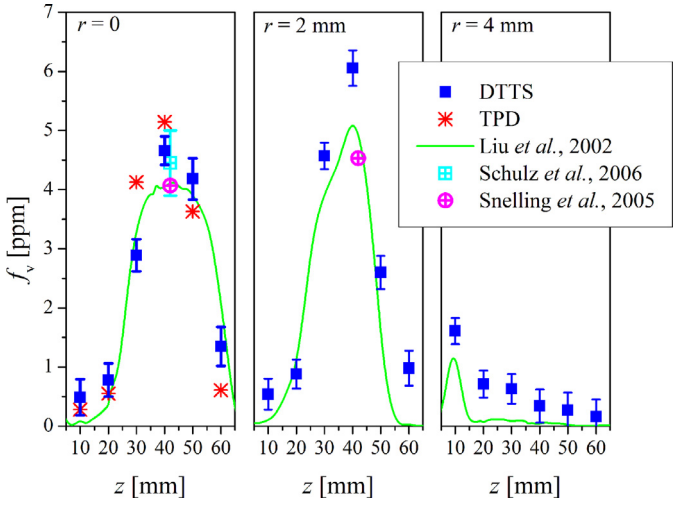

Fig. 7. Multi comparisons of soot volume fraction (f_v) measured by different techniques. Error bars of DTTS are calculated based on five independent tests at each sampling position.

4.3. Soot volume fraction

The soot volume fractions measured by DTTS at different sampling positions are compared with the experimental profiles that come from invasive TPD method and noninvasive laser-optical technique. As shown in Fig. 7, the spatial distributions of soot volume fraction are in qualitative and trend agreement with the laser extinction (LE)/Abel inversion technique by Liu et al. [16], and the data of DTTS is relatively higher than that of LE in most instances. The soot volume fraction on the flame centerline previously measured by TPD method is also included in the comparisons, in which the thermocouple employed in the experiment is the same as the design presented by McEnally et al. [26] The TPD gives the values between that of LE and DTTS at the two bottom locations, and yields overestimation at two middle ones as well as undervaluation at the top two ones. In addition, many LII experimental results from different researcher at a well-characterized position (42 mm above burner exit), as summarized by Schulz et al. [20], in which the soot volume fraction has a general range from 3.9 to 5.0 ppm, cover the DTTS data nearby locations. The soot volume fractions

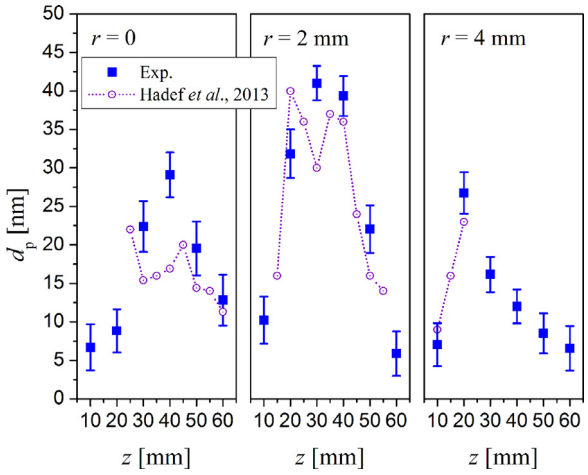

Fig. 8. Soot primary particle diameter profiles for some axial locations. Error bars are calculated based on five independent tests at each sampling position.

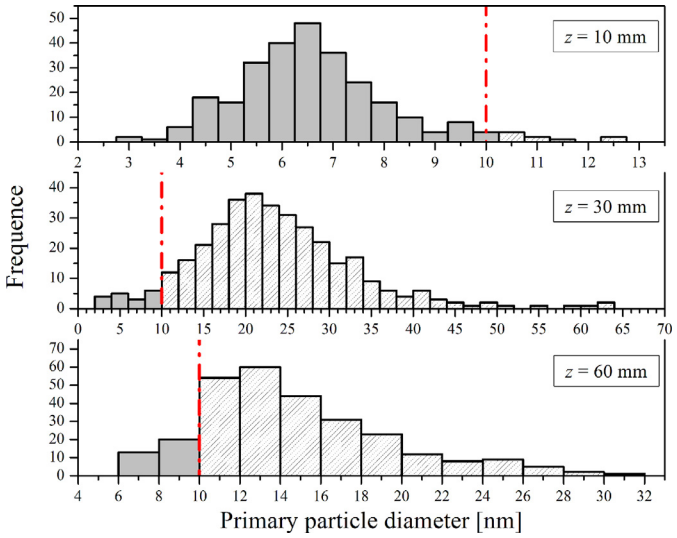

Fig. 9. Statistical histograms of primary particle diameter on the flame centerline (HAB = 10, 30 and 60 mm).

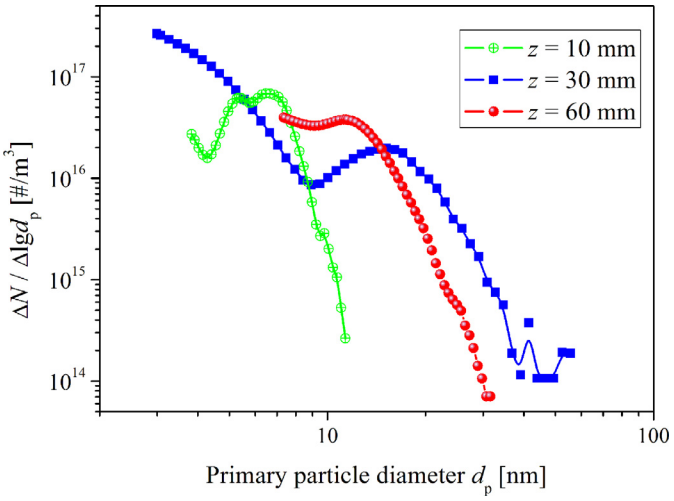

Fig. 10. Soot primary particle size distribution at three typical sampling points along the flame centerline (HAB = 10, 30 and 60 mm).

obtained from two laser techniques LII [48] and LE agree well with each other at the two positions (z=42 mm, r=0; r=2 mm).

The soot volume fractions are determined using TPD method and laser-optical techniques respectively based on a certain particle property assumption of bulk density and refractive index [26,33], whereas DTTS method can measure absolute soot volume fraction without requiring a prior knowledge of these particle properties. Electron microscopy images have showed that soot particle shape can change from spheres to fractal aggregates with polydispersion caused by coagulation processes and surface-growth reactions at increasing heights above the burner [20]. Therefore, the particle size and aggregate microstructure lead to substantial uncertainties of particle bulk density and refractive index, which could explain the discrepancy between DTTS method and TPD as well as laser methods. Another possible explanation for this difference among these methods is that the size of aggregates influences the thermophoretic velocity, and larger aggregates will deposit more rapidly than smaller ones on the sampling probe [49,50]. In this study, the assumption that the thermophoretic velocity is independent of the size of soot particles continues to be employed, which offers an opportunity to dramatically simplify the measurement and analysis. As shown in Fig. 7, the measurement result of particle volume fraction is higher than the benchmark value in the region of large aggregates, which can be attributed to the effect of aggregates size.

4.4. Soot particle size distribution

Figure 8 displays the mean diameter of soot primary particle at various HABs, in which DTTS measurements are compared with the results of LII [51]. The FESEM images of DTTS samples are analyzed using the ImageJ software to obtain the primary particle diameters. The primary particle diameters measured by image analysis cover a range of 3–100 nm, being in good agreement with LII results at intermediate HABs where soot particle size is dominated by growth. Whereas the LII measurements almost miss the data of small particles less than 10 nm in the bottom and tip of flame where soot inception and oxidation occur respectively. However, sub-10 nm particles can be effectively observed and counted by FESEM image analysis (as shown in Fig. S5 and Fig. S6 in SM), and thereby the DTTS is a reliable technique to detect the entire size distribution as soot particles evolve from nascent precursors to mature aggregates in flame.

Most of the experimental and numerical efforts focus on the mean attributes of particle population, such as soot volume fraction, number concentration and average size [52]. To improve our insight into soot phenomena, more elaborate investigates are needed to measure the detailed particle size distribution (PSD). Statistical histograms of primary particle diameter are determined from FESEM images of the soot samples collected at HAB = 10, 30 and 60 mm. As shown in Fig. 9, the polydisperse particle populations display patterns similar to log-normal distribution functions, in which the geometric standard deviations respectively are 1.26, 14.1 and 13.0. At the lowest flame location (z = 10 mm), the sub-10 nm particles make up the majority of soot volume with the percentage of 82.3%, while the middle and the highest locations just have the low proportion of 0.09% and 1.5%. This finding indicates that the soot volume fractions will agree better if small particles are exhaustively detected by laser techniques, especially in enrichment region of small particles due to soot inception and oxidation. Thus, the DTTS method possesses a significant advantage over other available diagnostics because it can analyze complete particle size spectrum.

In Fig. 10, the three PSDs are derived from the statistical histograms of primary particle diameter and corresponding soot volume fraction. It can be seen that the soot PSDs show bimodal

and even trimodal distributions. The bimodal PSD has a noticeable trough that separates the nucleation tail into the small size and log-normal like mode. At HAB = 10 mm, a trimodal PSD consists of one tail and two peaks, in which the tail and the first peak imply soot nucleation and surface-growth processes, and the second one might be associated with particle aggregation. Soot PSDs from unimodal to multimodal in laminar premixed flames have been found in several experimental studies [53]; however, there are few reports with respect to PSDs in soot laminar diffusion flames. Thus, these results are contributed to the soot community in favor of further research works.

5. Conclusions

In this paper, a practical sampling technique named dual exposure-time thermophoretic sampling (DTTS) is used to measure multiple parameters of sooting flame. The DTTS method possesses the superiority in simplicity and convenience, yielding spatially resolved stream velocities, soot volume fractions and soot particle sizes directly. The measurement does not depend on the prevailing seed-particle tracer, soot particle size, morphology, or optical characteristics. Most of all, the tailor-made UQGSs as thermophoresis probes can realize heat convection dominant due to effective insulation for heat radiation between flame and UQGS as well as little heat conduction loss. Therefore, the dynamic evolution of probe temperature conforms to first-order response equation, which provides a bridge between gas flow and soot particle thermophoresis. The unknown bivariate, flow velocity and soot volume fraction, are attained by double sampling with different exposure time intervals. By FESEM image analysis, the size distribution of primary particles within aggregates is obtained. Based on this measurement method, sufficient information about the flow field and particle population is attained, which is extremely valuable for researching and understanding the transport and dynamic evolution processes of soot particles.

Acknowledgments

This research was funded by National Natural Science Foundation of China (51522603, 51606079 and 51676078), China Postdoctoral Science Foundation (2016M592331) and the Foundation of State Key Laboratory of Coal Combustion (FSKLCCB1403). The authors are grateful to the Analytical and Testing Center of HUST for FESEM characterization of soot particles.

Supplementary materials

Supplementary material associated with this article can be found, in the online version, at doi:10.1016/j.combustflame.2017.03.003.

References

[1] T.H. Fletcher, J. Ma, J.R. Rigby, A.L. Brown, B.W. Webb, Soot in coal combustion systems, Prog. Energy Combust. Sci. 23 (1997) 283–301.
[2] A.E. Karataş, Ö.L. Gülder, Soot formation in high pressure laminar diffusion flames, Prog. Energy Combust. Sci. 38 (2012) 818–845.
[3] D.R. Tree, K.I. Svensson, Soot processes in compression ignition engines, Prog. Energy Combust. Sci. 33 (2007) 272–309.
[4] M. Commodo, G. De Falco, A. Bruno, C. Borriello, P. Minutolo, A. D'Anna, Physicochemical evolution of nascent soot particles in a laminar premixed flame: from nucleation to early growth, Combust. Flame 162 (2015) 3854–3863.
[5] S.B. Dworkin, Q. Zhang, M.J. Thomson, N.A. Slavinskaya, U. Riedel, Application of an enhanced PAH growth model to soot formation in a laminar coflow ethylene/air diffusion flame, Combust. Flame 158 (2011) 1682–1695.
[6] D. Chen, Z. Zainuddin, E. Yapp, J. Akroyd, S. Mosbach, M. Kraft, A fully coupled simulation of PAH and soot growth with a population balance model, Proc. Combust. Inst. 34 (2013) 1827–1835.
[7] H.-B. Zhang, X. You, H. Wang, C.K. Law, Dimerization of polycyclic aromatic hydrocarbons in soot nucleation, J. Phys. Chem. A 118 (2014) 1287–1292.
[8] E.K.Y. Yapp, C.G. Wells, J. Akroyd, S. Mosbach, R. Xu, M. Kraft, Modelling PAH curvature in laminar premixed flames using a detailed population balance model, Combust. Flame 176 (2017) 172–180.
[9] I.M. Kennedy, Models of soot formation and oxidation, Prog. Energy Combust. Sci. 23 (1997) 95–132.
[10] M.D. Smooke, M.B. Long, B.C. Connelly, M.B. Colket, R.J. Hall, Soot formation in laminar diffusion flames, Combust. Flame 143 (2005) 613–628.
[11] H. Wang, Formation of nascent soot and other condensed-phase materials in flames, Proc. Combust. Inst. 33 (2011) 41–67.
[12] A. Khosousi, F. Liu, S.B. Dworkin, N.A. Eaves, M.J. Thomson, X. He, Y. Dai, Y. Gao, F. Liu, S. Shuai, J. Wang, Experimental and numerical study of soot formation in laminar coflow diffusion flames of gasoline/ethanol blends, Combust. Flame 162 (2015) 3925–3933.
[13] M.L. Botero, E.M. Adkins, S. González-Calera, H. Miller, M. Kraft, PAH structure analysis of soot in a non-premixed flame using high-resolution transmission electron microscopy and optical band gap analysis, Combust. Flame 164 (2016) 250–258.
[14] J. Camacho, C. Liu, C. Gu, H. Lin, Z. Huang, Q. Tang, X. You, C. Saggese, Y. Li, H. Jung, L. Deng, I. Wlokas, H. Wang, Mobility size and mass of nascent soot particles in a benchmark premixed ethylene flame, Combust. Flame 162 (2015) 3810–3822.
[15] C.P. Arana, M. Pontoni, S. Sen, I.K. Puri, Field measurements of soot volume fractions in laminar partially premixed coflow ethylene/air flames, Combust. Flame 138 (2004) 362–372.
[16] F. Liu, H. Guo, G.J. Smallwood, Ö.L. Gülder, Effects of gas and soot radiation on soot formation in a coflow laminar ethylene diffusion flame, J. Quant. Spectrosc. Radiat. 73 (2002) 409–421.
[17] M.Y. Choi, A. Hamins, G.W. Mulholland, T. Kashiwagi, Simultaneous optical measurement of soot volume fraction and temperature in premixed flames, Combust. Flame 99 (1994) 174–186.
[18] C.R. Shaddix, K.C. Smyth, Laser-induced incandescence measurements of soot production in steady and flickering methane, propane, and ethylene diffusion flames, Combust. Flame 107 (1996) 418–452.
[19] B. Mewes, J.M. Seitzman, Soot volume fraction and particle size measurements withlaser-induced incandescence, Appl. Opt. 36 (1997) 709–717.
[20] C. Schulz, B.F. Kock, M. Hofmann, H. Michelsen, S. Will, B. Bougie, R. Suntz, G. Smallwood, Laser-induced incandescence: recent trends and current questions, Appl. Phys. B 83 (2006) 333.
[21] H.A. Michelsen, C. Schulz, G.J. Smallwood, S. Will, Laser-induced incandescence: particulate diagnostics for combustion, atmospheric, and industrial applications, Prog. Energy Combust. Sci. 51 (2015) 2–48.
[22] S. De Iuliis, M. Barbini, S. Benecchi, F. Cignoli, G. Zizak, Determination of the soot volume fraction in an ethylene diffusion flame by multiwavelength analysis of soot radiation, Combust. Flame 115 (1998) 253–261.
[23] D.R. Snelling, K.A. Thomson, G.J. Smallwood, L. Oslash, G-uacute lder, E.J. Weckman, R.A. Fraser, Spectrally resolved measurement of flame radiation to determine soot temperature and concentration, AIAA J. 40 (2002) 1789–1795.
[24] C. Lou, C. Chen, Y. Sun, H. Zhou, Review of soot measurement in hydrocarbon–air flames, Sci. China Technol. Sci. 53 (2010) 2129–2141.
[25] G.J. Nathan, P.A.M. Kalt, Z.T. Alwahabi, B.B. Dally, P.R. Medwell, Q.N. Chan, Recent advances in the measurement of strongly radiating, turbulent reacting flows, Prog. Energy Combust. Sci. 38 (2012) 41–61.
[26] C.S. McEnally, Ü.Ö. Köylü, L.D. Pfefferle, D.E. Rosner, Soot volume fraction and temperature measurements in laminar nonpremixed flames using thermocouples, Combust. Flame 109 (1997) 701–720.
[27] A.D. Eisner, D.E. Rosner, Experimental studies of soot particle thermophoresis in nonisothermal combustion gases using thermocouple response techniques, Combust. Flame 61 (1985) 153–166.
[28] Z. Xu, H. Zhao, Simultaneous measurement of internal and external properties of nanoparticles in flame based on thermophoresis, Combust. Flame 162 (2015) 2200–2213.
[29] Z. Xu, X. Tian, H. Zhao, Tailor-making thermocouple junction for flame temperature measurement via dynamic transient method, Proc. Combust. Inst. 36 (2017) 4443–4451.
[30] Z. Su, W. Zhou, Y. Zhang, New insight into the soot nanoparticles in a candle flame, Chem. Commun. 47 (2011) 4700–4702.
[31] A.P. George, R.D. Murley, E.R. Place, Formation of TiO_2 aerosol from the combustion supported reaction of $TiCl_4$ and O_2, Faraday Symp. Chem. Soc. 7 (1973) 63–71.
[32] R.A. Dobbins, C.M. Megaridis, Morphology of flame-generated soot as determined by thermophoretic sampling, Langmuir 3 (1987) 254–259.
[33] Ü.Ö. Köylü, C.S. McEnally, D.E. Rosner, L.D. Pfefferle, Simultaneous measurements of soot volume fraction and particle size / microstructure in flames using a thermophoretic sampling technique, Combust. Flame 110 (1997) 494–507.
[34] B.M. Kumfer, S.A. Skeen, R.L. Axelbaum, Soot inception limits in laminar diffusion flames with application to oxy–fuel combustion, Combust. Flame 154 (2008) 546–556.
[35] J.H. Frank, P.A.M. Kalt, R.W. Bilger, Measurements of conditional velocities in turbulent premixed flames by simultaneous OH PLIF and PIV, Combust. Flame 116 (1999) 220–232.
[36] R.M. Huffaker, Laser doppler detection systems for gas velocity measurement, Appl. Opt. 9 (1970) 1026–1039.
[37] A.M. Vargas, Ö.L. Gülder, A multi-probe thermophoretic soot sampling system for high-pressure diffusion flames, Rev. Sci. Instrum. 87 (2016) 055101.

[38] D.R. Snelling, K.A. Thomson, G.J. Smallwood, Ö.L. Gülder, Two-dimensional imaging of soot volume fraction in laminar diffusion flames, Appl. Opt. 38 (1999) 2478–2485.
[39] Ö.L. Gülder, K.A. Thomson, D.R. Snelling, Effect of fuel nozzle material properties on soot formation and temperature field in coflow laminar diffusion flames, Combust. Flame 144 (2006) 426–433.
[40] M. Balat-Pichelin, V.L. Kovalev, A.F. Kolesnikov, A.A. Krupnov, Effect of the incomplete accommodation of the heterogeneous recombination energy on heat fluxes to a quartz surface, Fluid Dyn 43 (2008) 830–838.
[41] Ü.Ö. Köylü, G.M. Faeth, T.L. Farias, M.G. Carvalho, Fractal and projected structure properties of soot aggregates, Combust. Flame 100 (1995) 621–633.
[42] S. Whitaker, Forced convection heat transfer correlations for flow in pipes, past flat plates, single cylinders, single spheres, and for flow in packed beds and tube bundles, AIChE J. 18 (1972) 361–371.
[43] D. Bradley, K.J. Matthews, Measurement of high gas temperatures with fine wire thermocouples, J. Mech. Eng. Sci. 10 (1968) 299–305.
[44] K.K. Kuo, Principles of combustion, 2nd ed., John Wiley, Hoboken, 2005, pp. 293–327.
[45] K.M. Leung, R.P. Lindstedt, W.P. Jones, A simplified reaction mechanism for soot formation in nonpremixed flames, Combust. Flame 87 (1991) 289–305.
[46] F. Liu, G.J. Smallwood, Ö.L. Gülder, Band lumping strategy for radiation heat transfer calculations using a narrowband model, J. Thermophys. Heat Transfer 14 (2000) 278–281.
[47] J. Lee, I. Altman, M. Choi, Design of thermophoretic probe for precise particle sampling, J. Aerosol Sci. 39 (2008) 418–431.
[48] D.R. Snelling, G.J. Smallwood, F. Liu, Ö.L. Gülder, W.D. Bachalo, A calibration-independent laser-induced incandescence technique for soot measurement by detecting absolute light intensity, Appl. Opt. 44 (2005) 6773–6785.
[49] D.W. Mackowski, Monte Carlo simulation of hydrodynamic drag and thermophoresis of fractal aggregates of spheres in the free-molecule flow regime, J. Aerosol Sci. 37 (2006) 242–259.
[50] E. Brugière, F. Gensdarmes, F.X. Ouf, J. Yon, A. Coppalle, Increase in thermophoretic velocity of carbon aggregates as a function of particle size, J. Aerosol Sci. 76 (2014) 87–97.
[51] R. Hadef, K. Geigle, J. Zerbs, R. Sawchuk, D. Snelling, The concept of 2D gated imaging for particle sizing in a laminar diffusion flame, Appl. Phys. B 112 (2013) 395–408.
[52] P. Akridis, S. Rigopoulos, Modelling of soot formation in laminar diffusion flames using a comprehensive CFD-PBE model with detailed gas-phase chemistry, Combust. Theor. Model (2016) 1–14.
[53] H. Mätzing, W. Baumann, H. Bockhorn, H.-R. Paur, H. Seifert, Detection of electrically charged soot particles in laminar premixed flames, Combust. Flame 159 (2012) 1082–1089.